Icarus 367 (2021) 114559

Contents lists available at ScienceDirect

Icarus

journal homepage: www.elsevier.com/locate/icarus

Note

The morphology and age of the Iapetus equatorial ridge supports an exogenic origin

Charlene E. Detelich [a,b,*], Paul K. Byrne [a], Andrew J. Dombard [c], Paul M. Schenk [d]

[a] Planetary Research Group, Department of Marine, Earth, and Atmospheric Sciences, North Carolina State University, Raleigh, NC 27695, USA
[b] Department of Geological Sciences, University of Alaska Anchorage, Anchorage, AK 99508, USA
[c] Department of Earth and Environmental Sciences, University of Illinois at Chicago, Chicago, IL 60607, USA
[d] Lunar and Planetary Institute, Universities Space Research Association, Houston, TX 77058, USA

ARTICLE INFO

Keywords:
Iapetus
Equatorial ridge
Geomorphology
Icy satellite
Craters

ABSTRACT

Both endogenic and exogenic formation mechanisms have been proposed for the equatorial ridge on Saturn's moon Iapetus. With photogeological mapping and crater statistics, we find that the morphology of the ridge is best explained by an exogenic origin, principally by the accretion onto the moon's surface of an orbiting ring of material.

1. Introduction

The Voyager flybys of the Saturnian system in 1980 and 1981 indicated the presence of enormous, isolated mountains on the icy moon Iapetus (Denk et al., 2000). Later observations by the Cassini mission revealed these mountains to be part of a striking ridge situated almost exactly at the equator (Porco et al., 2005). In places, this ridge is up to 20 km high and 70 km wide, and discontinuously spans almost 75% of the moon's circumference (Dombard et al., 2012; Giese et al., 2008; Kuchta et al., 2015; Lopez Garcia et al., 2014; Porco et al., 2005; Schenk et al., 2011; Singer and McKinnon, 2011). The moon itself also features 33.6 km of polar flattening (not including the equatorial ridge), such that the body has an equilibrium figure appropriate to a rotational period of ~16 h rather than its present-day period of 79.33 days (Thomas, 2010), although this oblate shape might not represent a frozen rotational bulge (Kay and Dombard, 2018). Further, the leading and trailing hemispheres of Iapetus have drastically different albedos, hypothesized to be the result of water ice sublimation from the leading hemisphere (Denk et al., 2010).

Numerous endogenic and exogenic formation mechanisms have been proposed for the origin of the ridge. Endogenic processes include tidal spindown (Castillo-Rogez et al., 2007; Porco et al., 2005; Roberts and Nimmo, 2009), convection (Czechowski and Leliwa-Kopystyński, 2008), despinning coupled with global volume change (Beuthe, 2010), global contraction (Sandwell and Schubert, 2010), or even intrusion (Melosh and Nimmo, 2009), although none of these mechanisms explains fully the location and morphology of the ridge (Schenk et al., 2011; Dombard et al., 2012). An exogenic origin for the ridge has been attributed to infall of a former Iapetian orbital ring (Ip, 2006; Levison et al., 2011) formed either by a destroyed subsatellite (Dombard et al., 2012), or by a giant impact coincident with despinning (Kuchta et al., 2015). The ring infall hypothesis was challenged by Giese et al. (2008); these authors suggested that, because the flanks of the equatorial ridge are less steep than the angle of repose, an exogenic origin is not plausible. However, formation of the ridge by some infall scenario was found possible by Lopez Garcia et al. (2014). Considering only endogenic ridge-formation mechanisms, Singer and McKinnon (2011) did not find a likely tectonic (or volcanic) origin for this landform.

The hypothesis that most closely matches observations of Iapetus and its ridge is that the moon had an ancient ring system that accreted onto the surface over time (e.g., Dombard et al., 2012; Stickle and Roberts, 2018). This hypothesis has been bolstered by previous studies of crater size–frequency distributions (CSFD), which showed that the ridge may be younger than the rest of the moon, consistent with an exogenic origin (Rivera-Valentín et al., 2014; Damptz et al., 2018). With imagery and topography based on that imagery, we characterized the morphology of the equatorial ridge and conducted additional CSFD analyses to test existing hypotheses of an exogenic origin for this enigmatic feature.

* Corresponding author at: Department of Geological Sciences, University of Alaska Anchorage, Anchorage, AK 99508, USA.
E-mail address: cedetelich@alaska.edu (C.E. Detelich).

https://doi.org/10.1016/j.icarus.2021.114559
Received 22 December 2020; Received in revised form 27 April 2021; Accepted 25 May 2021
Available online 28 May 2021

2. Methods

To assess its morphometry and map the spatial extent of the ridge, we used a global image mosaic of Iapetus, produced from Cassini Imaging Science Subsystem data, with a resolution of 400 m per pixel (m/px). With the mosaic base map, we identified and then recorded the approximate boundaries of the ridge as vector shapefiles with the ESRI® ArcMap™ 10.5 Geographical Information System (GIS) environment. With the Spatial Analyst and Field Calculator functions in ArcMap, we then found length and areal values for the mapped extent of the ridge, which were 3432 km and 416,477 km^2, respectively. We next used a global digital elevation model (DEM) (Schenk, 2010) with a resolution of 1 km/px, to take 83 cross-sectional profiles, each 40 km long, of the ridge at 300-km increments. We then plotted the maximum ridge relief with respect to longitude to characterize changes in ridge morphology around Iapetus.

For estimating the relative ages of a given region on Iapetus (we describe our study sites below), we performed CSFD analyses of eleven sites, deriving $N(D)$ values for each (where N is the number of craters of diameter D or greater per unit area—in this case, 1×10^6 km^2) (Crater Analysis Techniques Working Group, 1979). Stated errors are the standard deviation of a Poisson distribution, which is the square root of the number of craters per diameter bin per 10^6 km^2 (Michael et al., 2016). Although Iapetus does not likely host a substantial population of secondary craters (e.g., Bierhaus et al., 2012), we nonetheless excluded craters below five kilometers in diameter from our counts. The available image resolution of the Iapetus global mosaic challenges the positive identification of craters smaller than ~5 km in diameter (Wang et al., 2020) and undercounts of craters <5–10 km in diameter affect crater count statistics (Damptz et al., 2018).

Under the assumption that a greater CSFD value corresponds to an older age, an exogenic ridge that formed sometime after the moon itself should have lower $N(D)$ values than the surrounding terrain. However, we note that the deorbiting ring of material hypothesis represents an increased impactor flux, albeit at very small sizes, so this assumption may not be true for all crater diameters (Damptz et al., 2018). Regardless, considering that we excluded craters below a certain diameter threshold (5 km), the assumption that a greater CSFD value corresponds to an older age has been applied for this study. Conversely, similar $N(D)$ values for both the ridge and the rest of the moon would support either an endogenic origin for the landform, or that the accretion of a ring occurred very early. Crater statistics were obtained with the CraterTools extension (Kneissl et al., 2011) for ArcGIS 10.5, from the image base map described above.

We selected eleven areas on Iapetus as study sites for which to derive crater statistics (Fig. 1). One of the sites encompasses virtually the entire ridge itself and returns a representative value for the ridge independent of longitude. If the ridge were exogenic in origin, it stands that the landform would be less heavily cratered (and thus younger) than the surrounding plains. Another study site is an aggregate of five portions of the equator where no ridge appears present; we included these areas to determine whether the ridge simply did not form in these areas, or whether it did form but was not preserved there. The remaining nine sites were picked to ensure a broadly even geographic distribution between the leading and trailing hemispheres, influenced by the illumination geometry conditions under which component images of the global mosaic base map were acquired. Two of these nine study sites correspond to the floors of the Turgis and Engelier impact basins and are labled with site numbers 4 and 7, respectively.

3. Results

3.1. Ridge morphology

Our survey indicated that the equatorial ridge is non-continuous and encircles about 74% of Iapetus's equatorial region (Fig. 2a), a finding consistent with previous studies (e.g., Porco et al., 2005; Singer et al., 2012). In collating our topographic profiles, it appears that, with the data currently available, there is a notable difference in ridge morphology between the leading and trailing hemispheres, as had been noted by Schenk et al. (2011) and Castillo-Rogez et al. (2018). On the leading hemisphere, the ridge not only has greater maximum relief—19 km versus 8 km in the trailing hemisphere—but also has slightly steeper slopes. On the trailing hemisphere, the average ridge slope (as determined with limited topographic data) is 6° ± 4°. On the leading hemisphere, the ridge slopes vary between the Saturnian and anti-Saturnian

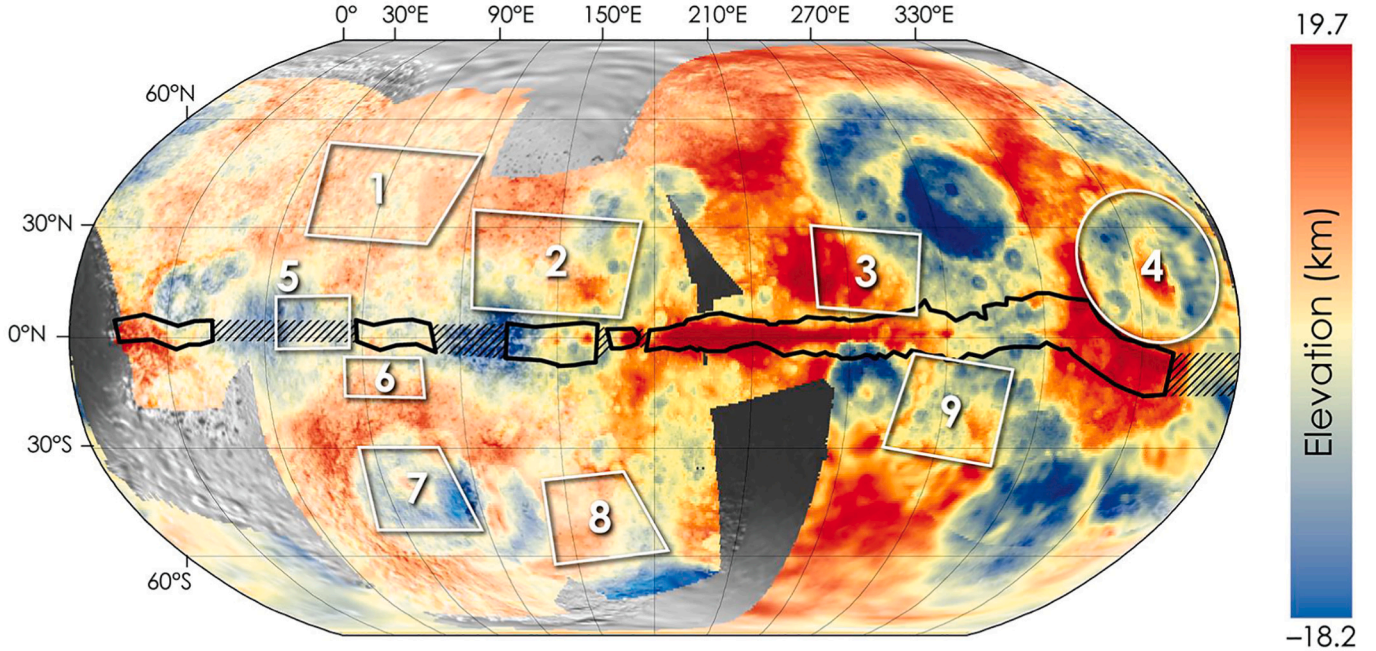

Fig. 1. The global topography for Iapetus overlain on the monochrome basemap, centered at 180°E and in Robinson projection. The white polygons and numbers denote our study sites; the ridge is outlined in a heavy black line, and hatching shows where the ridge is not visible (at least with presently available datasets).

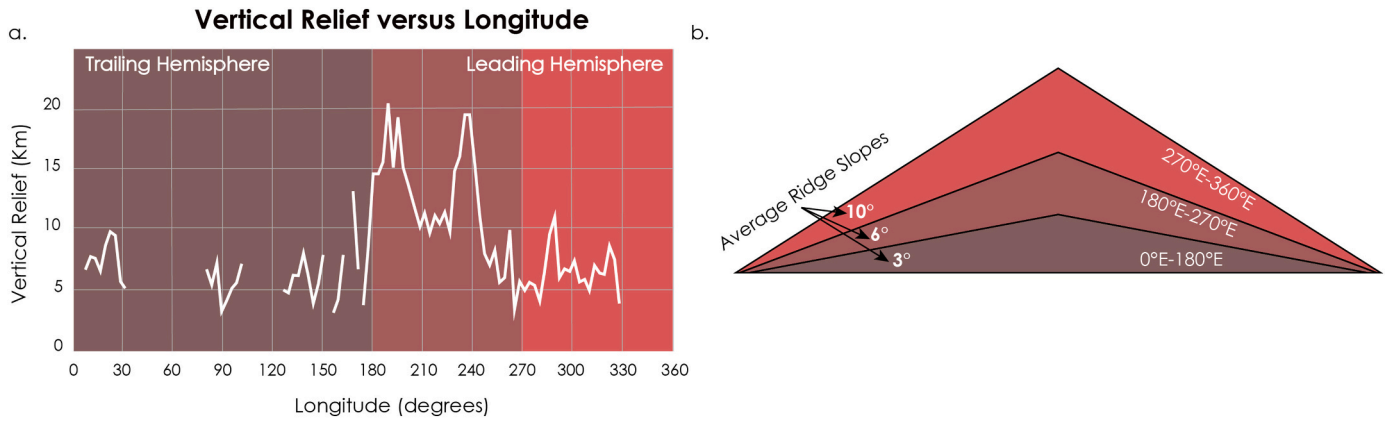

Fig. 2. (a) A plot of ridge relief (in km) with longitude. Gaps in the plot indicate regions where topographic data are not sufficient for resolving ridge morphometry. Available data indicate that ridge relief is substantially more pronounced on the leading hemisphere versus the trailing hemisphere of Iapetus. (b) A schematic of the contrast in ridge morphology between Iapetus's leading and trailing hemispheres. The values for average ridge slope are based on 83 cross-sectional profiles, each 40 km long and spaced at 300-km increments.

hemispheres (i.e., 180°E–270°E and 270°E–360°E, respectively). The average ridge slope from 180°E to 270°E is 10° ± 4°, whereas the average corresponding value from 270°E to 360°E is 4° ± 2°. These slope values are also consistent with those calculated by Lopez Garcia et al. (2014). By plotting ridge relief as a function of longitude, we found that the ridge is consistently taller on the leading hemisphere versus the trailing hemisphere. We also found that from 180°E to 270°E, the ridge is about twice as tall as it is from 270°E to 360° (Fig. 2b). Moreover, on the basis of available data, ridge material on the leading hemisphere is more spatially contiguous than on the trailing hemisphere. It is also important to note that the low albedo of the leading hemisphere facilitates more precise DEM calculations (White et al., 2013), and so relief values are likely more accurate for the leading hemisphere than for the trailing hemisphere.

3.2. Crater size–frequency distributions (CSFDs)

Our CSFD values for all eleven study sites are given in Fig. 3a. The ridge itself has average $N(10)$, $N(20)$, and $N(30)$ values of 519 ± 35, 113 ± 16, and 50 ± 11, respectively. Corresponding values for the aggregate areas where ridge material is not present (i.e., the apparently "missing" ridge sections) are 316 ± 50, 79 ± 25, and 39 ± 18. We found that, for some sites adjacent to the ridge (i.e., Sites 5, 6, and 9: Fig. 3c), CSFD values are greater for craters 20 km in diameter and above than corresponding values for the ridge itself (e.g., $N(20)$ of 198 ± 63 for Site 5 versus 113 ± 16 for the ridge). Site 3 has a greater $N(20)$ value (173 ± 38) than the ridge, but a lower $N(30)$ measure (33 ± 16 versus 50 ± 11); corresponding values for Site 4 are very close to those of the ridge (111 ± 22 and 53 ± 15, compared with 113 ± 16, and 50 ± 11, respectively). Of note, Sites 1 and 8 are both more cratered than the ridge, and are among the more distal locations we considered: $N(20)$ and $N(30)$ values for these two sites are 211 ± 38 and 95 ± 25, and 360 ± 66 and 156 ± 43, respectively. Site 7 has the lowest $N(10)$ and $N(20)$ values of any of the sites we considered (130 ± 39 and 24 ± 17, respectively), and hosts no superposed craters greater than 30 km in diameter. Per our counts, Site 2 (to the north of the ridge in the trailing hemisphere) has the fewest superposed craters of any of the sites we examined. Additionally, we note that $N(10)$ values are slightly greater on the leading hemisphere versus the trailing hemisphere, but this spatial variation in CSFD values is not apparent with the $N(20)$ and $N(30)$ values.

To test the null hypothesis that crater diameter data sets for each study site are unrelated to one another, we conducted two-sample *t*-tests. If the null hypothesis is supported, the *t*-test will return a *p*-value of >0.05. If the null hypothesis is rejected, the *t*-test will return a *p*-value of <0.05. We found that most crater diameter data sets have a *p*-value greater than >0.05 when compared with one another, and so are independent from one another at 95% confidence. The one exception to this finding was Site 3, for which $N(10)$ values are not independent to corresponding values for sites 1–6, 8, 9, and the "Ridge" and "Missing Ridge" sections. CSFD $N(20)$ values for Site 3 also returned a *p*-value <0.05 compared with $N(20)$ values for sites 2, 4, and 9, and the "Ridge" and "Missing Ridge" sections.

4. Discussion

Our morphological analysis indicates that most, by both volume and spatial footprint, of the ridge is situated on Iapetus's leading hemisphere (Fig. 2a). However, *some* of this observed hemispheric morphological dichotomy could reflect the effect of the dramatic differences in hemispheric albedo on Iapetus on derived DEM elevation values. Nonetheless, this asymmetry was previously noted by Schenk et al. (2011) and Castillo-Rogez et al. (2018). The difference in ridge volume between each hemisphere is considerable, although we did not find evidence with available data for flexure of the ice shell by this prominent landform (e.g., a linear moat beyond the base of the ridge in response to the ridge acting as a line load), as is observed around major lithospheric loads on other bodies (e.g., McGovern and Solomon, 1993). This lack of flexure indicates support of the ridge by a stiff lithosphere, suggesting that the ridge formed after the Iapetian ice shell thickened, and so is consistent with an exogenic origin for the feature (Dombard et al., 2012). Nonetheless, any endogenic process invoked for ridge formation must account not only for the morphology of the ridge, but for its apparently substantial spatial hemispheric asymmetry.

The difference in morphology between those portions of the ridge in the leading and trailing hemispheres may be a function of available data; globally contiguous, high-resolution imagery and topography, returned by a future mission to Iapetus, are required to fully test this possibility. Nonetheless, there appears to be a substantial contrast in how the equatorial ridge is manifest between hemispheres. It is not clear if the hemispherical contrast in ridge slope (Fig. 2b) denotes a particular geological property or process, although there is evidence for landslides along the ridge after formation (e.g., Singer et al., 2012). It may be, then, that the ridge segments in the trailing hemisphere, which have shallower slopes, have been more affected by mass wasting than that portion of the ridge on the leading hemisphere, potentially due to the presence of mechanically weaker or less consolidated material than in the leading hemisphere ridge. Detailed morphological mapping, such as that suggested by Stickle and Roberts (2018), could test this possibility—again, such mapping would benefit from improved data over those presently available.

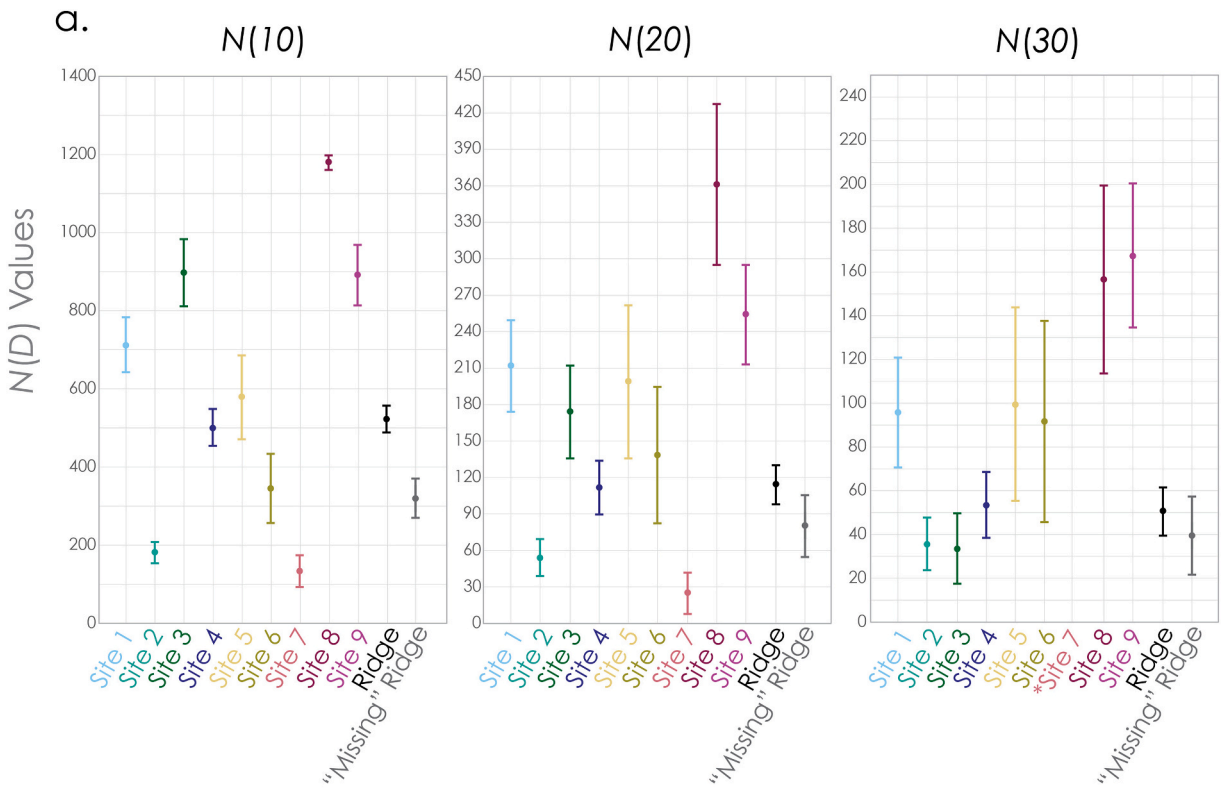

b.

Site	Area of Site
Site 1	147 × 10⁶ km²
Site 2	226 × 10⁶ km²
Site 3	122 × 10⁶ km²
Site 4	225 × 10⁶ km²
Site 5	50 × 10⁶ km²
Site 6	44 × 10⁶ km²
Site 7	85 × 10⁶ km²
Site 8	83 × 10⁶ km²
Site 9	150 × 10⁶ km²
Ridge	417 × 10⁶ km²
"Missing" Ridge	127 × 10⁶ km²

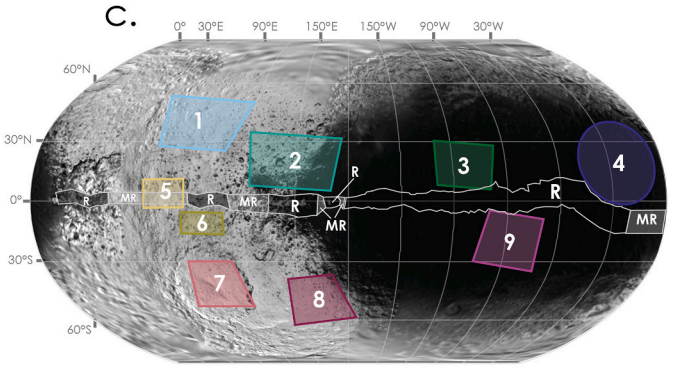

Fig. 3. a) $N(D)$ values (including error bars) for craters with diameters ≥10 km, ≥20 km, and ≥30 km. Site 7 does not possess any craters ≥30 km in diameter. b) A table of the areas of each study site. c) The crater counting sites overlain on the monochrome basemap, centered at 180°E and in Robinson projection. Sites labeled "R" correlate with the collective count area we designate "Ridge". Sites labeled "MR" denote "Missing Ridge".

Overall, our CSFD measurements indicate that the ridge is younger than its surroundings, on the basis of the greater number of craters in areas off the ridge than along the landform itself (Fig. 3a), a finding consistent with Damptz et al. (2018). For example, that Sites 3, 5, 6, and 9 have greater numbers of craters ≥20 km implies that they are older; we draw the same inference for Sites 1 and 8, which are more heavily cratered than the ridge at *all* diameters above 10 km. The similarity in CSFDs for Site 4 and the ridge is likely a function of the former corresponding to the floor of the Turgis basin (Fig. 3c); no ridge material crosses this 580-km-diameter basin, implying that the impact feature may have formed close in time with the ridge.

Although Site 7 is far from the ridge, its $N(20)$ and $N(30)$ values are considerably lower than those of the ridge because this part of Iapetus constitutes the floor of the 504-km-diameter Engelier basin; the basin interior is less cratered than much of the rest of the moon, and so is presumably younger than other portions of Iapetus's surface including the ridge (Fig. 1). (By implication, then, the Turgis basin formed before the Engelier impact.) It is not clear why Site 2 has anomalously low CSFD values, despite being situated far from the ridge. These data may reflect an apex–antapex asymmetry in cratering rates (e.g., Dones et al., 2009). Although this effect is not expected for craters ≤30 km in diameter (Hirata, 2016), this asymmetry is apparent in exactly the crater size range where we see the most obvious lack of craters (Fig. 3a).

We also determined that equatorial regions without ridge material (i.e., the areas of "Missing Ridge") are, in general, less heavily cratered and thus presumably younger than both their surroundings *and* the ridge. With the exception of the Turgis basin (and possibly the 244-km-diameter Naimon basin), places where the ridge is not present do not obviously correspond to impact sites. Yet these areas *are* generally topographically low: the equatorial area due south of Abisme basin (768 km in diameter) is part of a regional, linear low that strikes approximately northwest–southeast, and the two regions devoid of ridge material at 62°E and 130°E are situated in quasi-circular depressions, too (Fig. 1). If the ridge were formerly contiguous along all longitudes on

Iapetus, before portions therein were removed by impacts that correspond to the present-day equatorial lows, then those impacts must have occurred very early in Iapetus's history for their morphological signatures to be minimal today.

It is also possible, under a scenario where the ridge was deposited as a collapsed disk of ring material (Dombard et al., 2012; Ip, 2006; Kuchta et al., 2015; Levison et al., 2011), that the emplacement of such material could have been geographically uneven to the extent that little to no deposition occurred at some longitudes (Stickle and Roberts, 2018). Indeed, Stickle and Roberts (2018) found that such irregular deposition would be the rule, not the exception, given that accreting ring material would likely impact Iapetus at high incidence angles; this impacting would lead to positive topography (i.e., the ridge), with emplaced material forming discontinuous ridge segments and subsequently impacted material piling up behind initial deposits. Regardless of the exact manner in which exogenically derived material accumulated on Iapetus, it is unsurprising, then, that the ridge is not contiguous along the moon's equator.

5. Concluding remarks

In this study, we performed morphological and crater statistical analyses on the equatorial ridge of Iapetus to test the hypothesis for an exogenic origin for this distinctive landform. Our assessment of ridge morphology indicates that, although discontinuous along the Iapetian equator and subject to the quality of available data, the majority volume of the landform appears to be situated on the moon's leading hemisphere. This asymmetry extends to the shape and size of the ridge: the leading-hemisphere portions of the ridge are taller and steeper than those on the trailing hemisphere. On the basis of our CSFD measurements, the ridge is less heavily cratered and presumably younger than the surrounding plains, a result in agreement with previous studies (e.g., Damptz et al., 2018). Our study does not exclude fully the possibility of an endogenic origin for the ridge, but our findings are much more consistent with proposed formation mechanisms that invoke the infall of a former ring and/or disrupted satellite of Iapetus itself (e.g., Ip, 2006; Dombard et al., 2012) than with any interior process. Further, the absence of ridge material at certain points along the equator can be accounted for by the irregular accretion of ring material in stages (Stickle and Roberts, 2018)—although some sites where the ridge is absent are regional topographic lows, and so the possibility of early impact-driven removal of ring deposits cannot be excluded.

Nonetheless, a view is emerging that the Iapetian ridge is not the result of interior processes but instead reflects the collision of formerly orbiting material about the moon (Damptz et al., 2018), probably at incident angles sufficiently high so as to avoid both substantial removal of topography and heating of the icy surface (Stickle and Roberts, 2018). In fact, such an accretionary mechanism might account not only for the Iapetian equatorial ridge, but also for the moon's oblate shape itself (Leleu et al., 2018). Although it does not have a topographic expression, Rhea, another Saturnian moon, has an equatorial feature termed the "blue circle" (Schenk et al., 2011). Somewhat similar ridge-like features are also present along the equators of the Saturnian irregular moonlets Pan and Atlas; these ridges may correspond to piles of Saturn ring particles that accreted after the satellites had formed (e.g., Charnoz et al., 2007). An equatorial ridge-like feature is also present on near-Earth asteroids 66391 Moshup (1999 KW4) (Ostro et al., 2006), Bennu (101955), and Ryugu (162173) (Hirabayashi et al., 2020). However, ridges on these small bodies are attributed to rotation near the critical state. This type of feature would not occur on a self-gravitating body such as Iapetus as the body of the moon would bifurcate into a triaxial ellipsoid instead of forming an equatorial feature (Dombard et al., 2012).

Even with growing evidence for an exogenic origin of the ridge, several important questions remain. For example, the nature of the "Missing Ridge" portions along Iapetus's equator is unclear: are these ancient impact sites, or happenstance areas where no impacting ring material was deposited? The apparent difference in ridge slope between the leading and trailing hemispheres is also puzzling; if the entire volume of ridge material were to have uniform mechanical properties, it follows that the angle of repose should not vary along the length of the landform. The absolute age of the ridge remains unknown, yet is key to further distinguishing endogenic from exogenic formation scenarios (Damptz et al., 2018). Continued work to characterize the crater production function within the Saturnian system (e.g., Kirchoff and Schenk, 2010), together with high-resolution image and topographic data from future exploration of Iapetus, would provide important and still much-needed constraints on how the Iapetian ridge formed.

Declaration of Competing Interest

The authors declare that they have no known competing financial interests or personal relationships that could have appeared to influence the work reported in this paper.

Acknowledgements

CED and PKB acknowledge support from North Carolina State University. CED also acknowledges helpful conversations with Geoffrey Collins.

References

Beuthe, M., 2010. East–west faults due to planetary contraction. Icarus 209, 795–817.
Bierhaus, E.B., Dones, L., Alvarellos, J.L., Zahnle, K., 2012. The role of ejecta in the small crater populations on the mid-sized saturnian satellites. Icarus 218, 602–621.
Castillo-Rogez, J.C., Matson, D.L., Sotin, C., Johnson, T.V., Lunine, J.I., Thomas, P.C., 2007. Iapetus' geophysics: rotation rate, shape, and equatorial ridge. Icarus 190, 179–202.
Castillo-Rogez, J.C., Hemingway, D., Rhoden, A., Tobie, G., McKinnon, W.B., Dotson, R., 2018. Origin and evolution of Saturn's mid-sized moons. In: Schenk, P.M., Clark, R. N., Howett, C.J.A., Verbiscer, A.J., Waite, J.H. (Eds.), Enceladus and the Icy Moons of Saturn. University of Arizona Press, pp. 285–306.
Charnoz, S., Brahic, A., Thomas, P.C., Porco, C.C., 2007. The equatorial ridges of Pan and atlas: terminal accretionary ornaments? Science 318, 1622–1624.
Crater Analysis Techniques Working Group, 1979. Standard techniques for presentation and analysis of crater size-frequency data. Icarus 37, 467–474.
Czechowski, L., Leliwa-Kopystyński, J., 2008. The Iapetus's ridge: possible explanations of its origin. Adv. Space Res. 42, 61–69.
Damptz, A.L., Dombard, A.J., Kirchoff, M.R., 2018. Testing models for the formation of the equatorial ridge on Iapetus via crater counting. Icarus 302, 134–144.
Denk, T., et al., 2000. Iapetus (1): Size, topography, surface structures, craters. In: Presented at the 31st Lunar and Planetary Science Conference, Abstract #1596.
Denk, T., et al., 2010. Iapetus: unique surface properties and a global color dichotomy from Cassini imaging. Science 327, 435–439.
Dombard, A.J., Cheng, A.F., McKinnon, W.B., Kay, J.P., 2012. Delayed formation of the equatorial ridge on Iapetus from a subsatellite created in a giant impact. J. Geophys. Res.-Planet 117.
Dones, L., et al., 2009. Icy satellites of Saturn: Impact cratering and age determination. In: Dougherty, M.K., Esposito, L.W., Krimigis, S.M. (Eds.), Saturn from Cassini-Huygens. Springer Netherlands, Dordrecht, pp. 613–635.
Giese, B., et al., 2008. The topography of Iapetus' leading side. In: Icarus, Saturn's Icy Satellites from Cassini, 193, pp. 359–371.
Hirabayashi, M., et al., 2020. Spin-driven evolution of asteroids' top-shapes at fast and slow spins seen from (101955) Bennu and (162173) Ryugu. Icarus 352, 113946.
Hirata, N., 2016. Differential impact cratering of Saturn's satellites by heliocentric impactors. J. Geophys. Res.-Planet 121, 111–117.
Ip, W.-H., 2006. On a ring origin of the equatorial ridge of Iapetus. Geophys. Res. Lett. 33.
Kay, J.P., Dombard, A.J., 2018. Formation of the bulge of Iapetus through long-wavelength folding of the lithosphere. Icarus 302, 237–244.
Kirchoff, M.R., Schenk, P., 2010. Impact cratering records of the mid-sized, icy saturnian satellites. Icarus, Cassini at Saturn 206, 485–497.
Kneissl, T., van Gasselt, S., Neukum, G., 2011. Map-projection-independent crater size-frequency determination in GIS environments—new software tool for ArcGIS. Planet Space Sci., Geological Mapping of Mars 59, 1243–1254.
Kuchta, M., et al., 2015. Despinning and shape evolution of Saturn's moon Iapetus triggered by a giant impact. Icarus 252, 454–465.
Leleu, A., Jutzi, M., Rubin, M., 2018. The peculiar shapes of Saturn's small inner moons as evidence of mergers of similar-sized moonlets. Nat. Astr. 2, 555–561.
Levison, H.F., Walsh, K.J., Barr, A.C., Dones, L., 2011. Ridge formation and de-spinning of Iapetus via an impact-generated satellite. Icarus 214, 773–778.

Lopez Garcia, E.J., Rivera-Valentín, E.G., Schenk, P.M., Hammond, N.P., Barr, A.C., 2014. Topographic constraints on the origin of the equatorial ridge on Iapetus. Icarus 237, 419–421.
McGovern, P.J., Solomon, S.C., 1993. State of stress, faulting, and eruption characteristics of large volcanoes on Mars. J. Geophys. Res.-Planet 98, 23553–23579.
Melosh, H.J., Nimmo, F., 2009. An intrusive dike origin for Iapetus' enigmatic ridge?. In: Presented at the 40th Lunar and Planetary Science Conference, Abstract #2478, p. 2478.
Michael, G.G., Kneissl, T., Neesemann, A., 2016. Planetary surface dating from crater size-frequency distribution measurements: Poisson timing analysis. Icarus 277, 279–285.
Ostro, S.J., et al., 2006. Radar imaging of binary near-earth asteroid (66391) 1999 KW4. Science 314, 1276–1280.
Porco, C.C., et al., 2005. Cassini imaging science: initial results on Phoebe and Iapetus. Science 307, 1237–1242.
Rivera-Valentín, E.G., Barr, A.C., Garcia, E.J.L., Kirchoff, M.R., Schenk, P.M., 2014. Constraints on planetesimal disk mass from the cratering record and equatorial ridge on Iapetus. ApJ 792, 127.
Roberts, J.H., Nimmo, F., 2009. Tidal dissipation due to despinning and the equatorial ridge on Iapetus. In: Presented at the 40th Lunar and Planetary Science Conference, Abstract #1927.
Sandwell, D., Schubert, G., 2010. A contraction model for the flattening and equatorial ridge of Iapetus. Icarus 210, 817–822.
Schenk, P.M., 2010. Global topographic mapping of Saturn's midsize icy satellites: system-wide thermal and impact effects. In: Presented at the American Astronomical Society, DPS Meeting #42 id.9.16.
Schenk, P.M., et al., 2011. Plasma, plumes and rings: saturn system dynamics as recorded in global color patterns on its midsize icy satellites. Icarus 211, 740–757.
Singer, K.N., McKinnon, W.B., 2011. Tectonics on Iapetus: despinning, respinning, or something completely different? Icarus 216, 198–211.
Singer, K.N., McKinnon, W.B., Schenk, P.M., Moore, J.M., 2012. Massive ice avalanches on Iapetus mobilized by friction reduction during flash heating. Nat. Geosci. 5, 574–578.
Stickle, A.M., Roberts, J.H., 2018. Modeling an exogenic origin for the equatorial ridge on Iapetus. Icarus 307, 197–206.
Thomas, P.C., 2010. Sizes, shapes, and derived properties of the saturnian satellites after the Cassini nominal mission. Icarus 208, 395–401.
Wang, Y., Xie, M., Xiao, Z., Cui, J., 2020. The minimum confidence limit for diameters in crater counts. Icarus 341, 113645.
White, O.L., Schenk, P.M., Dombard, A.J., 2013. Impact basin relaxation on Rhea and Iapetus and relation to past heat flow. Icarus 223, 699–709.